

Bilayer Hubbard model for ${}^3\text{He}$: a cluster dynamical mean-field calculation

K. S. D. Beach⁽¹⁾ and F. F. Assaad⁽²⁾

⁽¹⁾*Department of Physics, University of Alberta, Edmonton, Alberta, Canada T6G 2G7*

⁽²⁾*Institut für theoretische Physik und Astrophysik, Universität Würzburg, Am Hubland, D-97074 Würzburg, Germany*

Inspired by recent experiments on bilayer ${}^3\text{He}$, we consider a bilayer Hubbard model on a triangular lattice. For appropriate model parameters, we observe a band-selective Mott transition at a critical chemical potential, μ_c , corresponding to the solidification of the fermions in the first layer. The growth of the effective mass on the metallic side ($\mu < \mu_c$) is cut off by a first order transition in which the first layer fermions drop out of the Luttinger volume and their spin degrees of freedom become locked in a spin singlet state. These results are obtained from a cluster dynamical mean-field calculation on an eight-site cluster with a quantum Monte Carlo cluster solver.

The solidification of ${}^3\text{He}$ monolayers [1] has been interpreted as a density-driven Mott transition in which the effective mass diverges [2, 3]. Below the critical density, the metallic phase corresponds to a nearly localized Fermi liquid and, beyond the critical density, to a spin-disordered solid. Recently, it has been possible to realize bilayers of ${}^3\text{He}$ [4] (atop a frozen ${}^4\text{He}$ substrate, itself adsorbed onto graphite) with the special property that the second layer begins to form before the first has solidified. Since the first layer is close to a Mott transition, the ${}^3\text{He}$ fermions in this layer are slow (i.e. heavy), whereas those in the second layer are fast. This combination of fast and slow dynamics—corresponding to wide and narrow fermion conduction bands—is completely analogous to the situation in electronic heavy fermion materials, albeit without the complication of crystal field and spin orbit effects.

According to this picture, prior to solidification of the first layer, one expects an enhanced effective mass and a Luttinger volume that counts both the first- and second-layer populations. Moreover, one naively anticipates that further ${}^3\text{He}$ deposition will eventually cause the effective mass to diverge. In experiment, the effective mass is indeed observed to increase as a function of the total ${}^3\text{He}$ concentration, but its growth is interrupted by an intervening phase [4] in which the first ${}^3\text{He}$ layer is a spin-disordered insulator, decoupled from the second layer.

The motivation for this Letter is to consider a simple lattice model that goes a good way toward reproducing the aforementioned experimental situation. As shown in Figs. 1(a) and 1(b), we adopt a *stacking of billiard balls* modeling of bilayer ${}^3\text{He}$ on a triangular lattice defined by $\mathbf{a}_1 = (1/2, \sqrt{3}/2, 0)$ and $\mathbf{a}_2 = (1, 0, 0)$. Each unit cell accounts for two ${}^3\text{He}$ positions, $\mathbf{r}_f = \mathbf{0}$ and $\mathbf{r}_c = \frac{2}{3}\mathbf{a}_1 - \frac{1}{3}\mathbf{a}_2 + (0, 0, a_3)$, measured relative to the lattice. Note that this presupposes a particular stacking arrangement for the second ${}^3\text{He}$ layer.

Our model can be viewed as a honeycomb lattice whose inequivalent sites (corresponding to ${}^3\text{He}$ positions in the upper and lower layers) are populated by two species of fermion, which we label c and f . The tight-binding parameters include a nearest-neighbour (interlayer) hopping V and next-nearest-neighbour (intralayer) hoppings

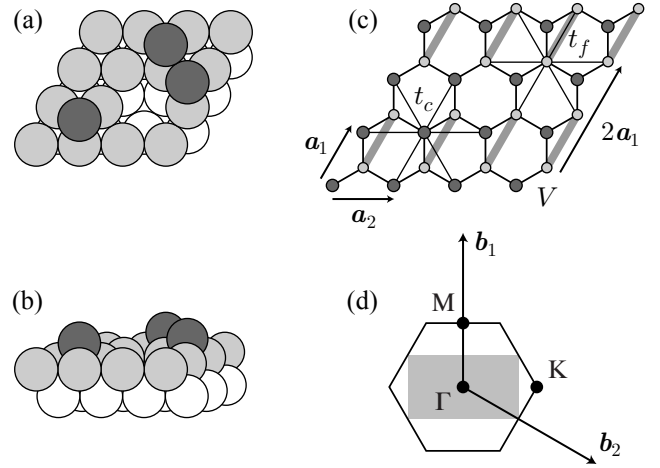


FIG. 1: (a),(b) Stacking of billiard balls modeling of bilayer ${}^3\text{He}$, top and side view, with the ${}^4\text{He}$ substrate shown in white. (c) Tight-binding modeling with hoppings t_c , t_f , and V . The grey bars connecting f fermion sites (first-layer ${}^3\text{He}$ positions) indicate a possible singlet pattern compatible with the eight-site $2\mathbf{a}_1 \times 2\mathbf{a}_2$ and four-site $2\mathbf{a}_1 \times \mathbf{a}_2$ unit cells. (d) The hexagonal Brillouin zone of the triangular lattice and the rectangular zone that results from the folding $\mathbf{b}_1 \rightarrow \frac{1}{2}\mathbf{b}_1$.

t_c and t_f . See Fig. 1(c). With the inclusion of onsite Coulomb repulsion terms, the Hamiltonian reads

$$H = \sum_{\mathbf{k}, \sigma} \begin{pmatrix} c_{\mathbf{k}, \sigma}^\dagger & f_{\mathbf{k}, \sigma}^\dagger \end{pmatrix} \begin{pmatrix} \varepsilon_c(\mathbf{k}) - \mu & V(\mathbf{k}) \\ V(\mathbf{k}) & \varepsilon_f(\mathbf{k}) - \mu \end{pmatrix} \begin{pmatrix} c_{\mathbf{k}, \sigma} \\ f_{\mathbf{k}, \sigma} \end{pmatrix} + U_c \sum_{\mathbf{i}} (\hat{n}_{c, \mathbf{i}} - 1)^2 + U_f \sum_{\mathbf{i}} (\hat{n}_{f, \mathbf{i}} - 1)^2. \quad (1)$$

Here, the mixing element $V(\mathbf{k}) = V(1 + \gamma_{\mathbf{k}})^{1/2}$ and the dispersion $\varepsilon_c(\mathbf{k}) = -t_c \gamma_{\mathbf{k}} + \varepsilon_c^0$ are expressed in terms of the connection $\gamma_{\mathbf{k}} = \cos(\mathbf{k} \cdot \mathbf{a}_1) + \cos(\mathbf{k} \cdot \mathbf{a}_2) + \cos[\mathbf{k} \cdot (\mathbf{a}_2 - \mathbf{a}_1)]$ of the underlying Bravais lattice. The operator $\hat{n}_{c, \mathbf{i}} = \sum_{\sigma} c_{\mathbf{i}, \sigma}^\dagger c_{\mathbf{i}, \sigma}$ is the local ${}^3\text{He}$ density in the upper layer. Similar definitions hold for $\varepsilon_f(\mathbf{k})$ and $\hat{n}_{f, \mathbf{i}}$.

Except for the complication of the layer stacking (and the resulting \mathbf{k} -dependent hybridization), this bilayer Hubbard model reduces to the Periodic Anderson Model

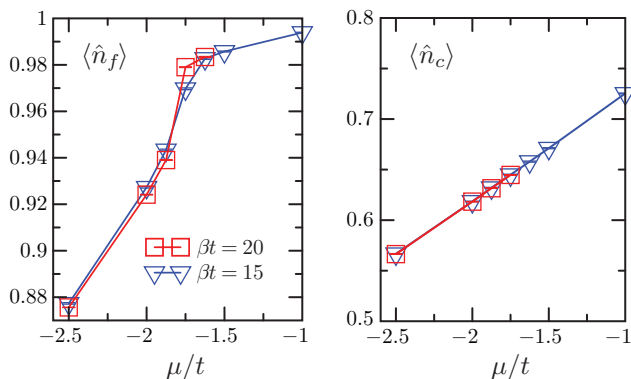


FIG. 2: Single particle occupation number for the f and c fermions as a function of temperature.

as $t_f \rightarrow 0$, a limit in which the bare mass of the f fermions diverges. Similar models (though ones with a somewhat unrealistic *direct* layer stacking) have been considered for the description of bilayer ^3He in Refs. 5 and 6 within a slave boson mean-field calculation. Here we go one step further and perform calculations within the cellular dynamical mean field theory (CDMFT) [7] approximation using a supercell defined by the lattice constants $L_c \mathbf{a}_1$ and $L_c \mathbf{a}_2$ with $L_c = 2$. Since the original unit cell contains two orbitals, this amounts to a total of eight orbitals per supercell. The resulting single particle Green function, $\underline{G}(\mathbf{K}, i\omega_m)$, is a $2L_c^2 \times 2L_c^2$ matrix with crystal momentum \mathbf{K} in the Brillouin zone of the supercell lattice. The CDMFT calculation involves neglecting momentum conservation and thereby obtaining a \mathbf{K} -independent self-energy $\underline{\Sigma}(i\omega_m)$. This quantity is extracted from an $L_c \times L_c$ cluster of unit cells embedded in a dynamical mean field that is determined self-consistently. We have solved this cluster problem using a standard Hirsch-Fye approach and have symmetrized the cluster Green function to obtain the corresponding quantity on the lattice:

$$G(\mathbf{k}, i\omega_m)_{\mu,\nu} = \frac{1}{L_c^2} \sum_{\alpha,\beta} e^{i\mathbf{k}\cdot(\mathbf{x}_\alpha - \mathbf{x}_\beta)} \underline{G}(\mathbf{K}, i\omega_m)_{(\mu,\alpha),(\nu,\beta)}. \quad (2)$$

Here \mathbf{x}_α denotes the unit cell positions within the supercell, μ and ν run over the c and f orbitals within each unit cell, and \mathbf{k} and \mathbf{K} differ by a reciprocal lattice vector of the supercell Bravais lattice. The rotation to real frequencies was carried out with a stochastic analytical continuation technique [8, 9].

We consider the following model parameters: $t_c = t_f = t$, $U_c/t = U_f/t = 12$, $V_0/t = 1/2$, $\varepsilon_c^0/t = 3$ and $\varepsilon_f^0/t = 0$. We have chosen large values of U_c and U_f to reflect the contact repulsion of the ^3He atoms and to guarantee that each single layer is well within the Mott insulating phase at half-band filling [10]. These values of the Hubbard interaction lead to low double occupancy, thus generating local moments. The difference $\varepsilon_c^0 - \varepsilon_f^0 > 0$ is a crude accounting for the van der Waals forces (both ^4He –

^3He and ^3He – ^3He) that preferentially fill the first layer. Fig. 2 plots the layer densities $\langle \hat{n}_f \rangle$ and $\langle \hat{n}_c \rangle$ as a function of the chemical potential, which controls the overall ^3He concentration. Analysis of the temperature dependence of $\langle \hat{n}_f \rangle$ is consistent with a zero-temperature jump of this quantity at $\mu = \mu_c \simeq -1.8t$. In contrast, $\langle \hat{n}_c \rangle$ increases smoothly with the chemical potential. Since $\frac{\partial F}{\partial \mu} = \langle \hat{n}_c + \hat{n}_f \rangle$, the jump in the total fermionic density signals a density-driven first order transition. In a canonical ensemble, states with total density lying within the jump are phase separated. The first order nature of this phase transition can be confirmed explicitly on smaller four-site clusters, which can be simulated at much lower temperatures before the negative sign problem becomes unmanageable [11].

The nature of the distinct metallic phases on either side of the transition is best understood in terms of the single particle spectral function,

$$A(\mathbf{k}, \omega) = -\text{Im Tr } G(\mathbf{k}, \omega), \quad (3)$$

plotted in Fig. 3. For $\mu < \mu_c$, and as exemplified by the data set at $\mu = -2.5t$, the low-energy coherent features of the spectral function compare favorably with a slave boson approximation leading to mass-renormalized, hybridized bands. This state has a Luttinger volume that includes both f and c fermions, and the band with the largest Fermi volume has dominant f character. As a function of the chemical potential, the effective mass of the f band grows; beyond μ_c , the f band drops out of the low-energy physics altogether. This can be understood at the *static* mean field level by a conventional slave boson theory in competition with local singlet formation in the first layer. The transition is signaled by the appearance of an anomalous expectation value $\Delta_{\mathbf{j}} \sim (t_f^2/U_f) \sum_{\sigma} \langle f_{\mathbf{i},\sigma}^\dagger f_{\mathbf{j},\sigma} \rangle$. The upper inset of Fig. 3 shows the band structure that results when this singlet order parameter has the configuration depicted in Fig. 1(c).

We understand this transition to be of the band-selective Mott type, in which a half-filled band with dominant f and sub-dominant c character is gapped beyond μ_c . This interpretation is supported by the fact that, beyond μ_c , $\langle \hat{n}_f \rangle$ does not saturate to unity, as in the case of an orbital-selective Mott transition [16]. The data in Fig. 3 show the typical Mott-Hubbard transfer of spectral weight from the upper band at $\omega \sim 6t$ ($\mu = -1.75t$) down to the Fermi energy as a function of decreasing chemical potential [12]. In the generic Mott-Hubbard scenario, doping occurs when the chemical potential reaches the lower Hubbard band, which in the present case is situated at roughly $\omega \sim -6t$ for $\mu = -1.75t$. In the band-selective Mott transition, doping is provided by changing the occupation of the ungapped band.

To accurately estimate the effective mass renormalization at $\mu < \mu_c$, we consider the self-energy, $\Sigma_{ff}(\mathbf{k}, \omega_m)$, as defined by $G_{ff}^{-1}(\mathbf{k}, i\omega_m) = i\omega_m - \varepsilon_f(\mathbf{k}) + \mu - \Sigma_{ff}(\mathbf{k}, \omega_m)$, with the Green function taken from Eq. (2). Since at

$\mu < \mu_c$ the self-energy is dominated by its frequency dependence, the effective mass renormalization is very well approximated by the inverse quasiparticle residue,

$$\frac{m^*}{m} \propto Z^{-1}(\mathbf{k}) = 1 - \left. \frac{\partial \text{Im} \Sigma_{ff}(\mathbf{k}, i\omega_m)}{\partial \omega_m} \right|_{\omega_m \rightarrow 0}. \quad (4)$$

This quantity is plotted in Fig. 4 for Fermi wave vectors of the f band along the Γ -M and K- Γ directions in the Brillouin zone. A monotonic increase of the effective mass is observed, but its divergence is preempted by the first order transition at $\mu = \mu_c$.

The growth of the effective mass corresponds to a decrease of the coherence temperature, T_{coh} , below which Fermi liquid behavior manifests itself. To illustrate this,

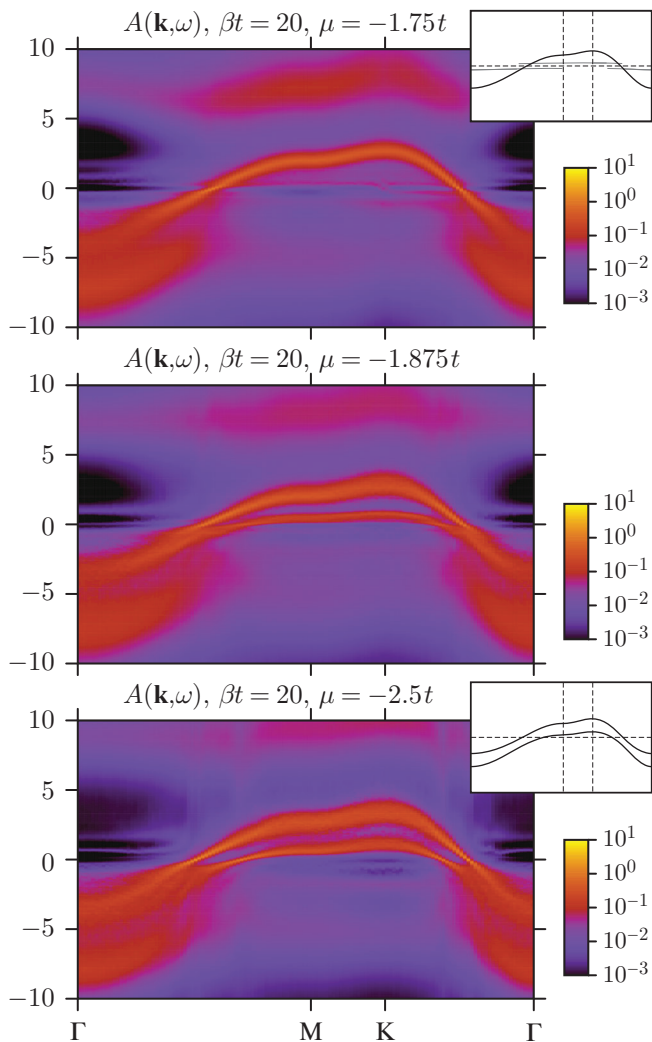


FIG. 3: The amplitude of the single particle spectral function, as defined by Eq. (3), is plotted for various values of the chemical potential. The lower inset shows the mean-field band structure consisting of two quasiparticle bands of mixed c and f character. The upper inset shows the single c -only band completely decoupled from the gapped, nearly flat band of the singlet-bound f fermions.

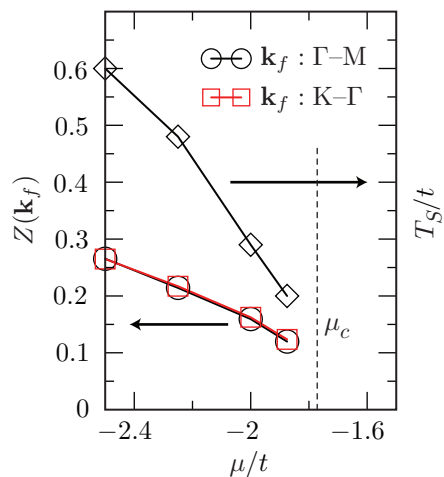


FIG. 4: Quasiparticle residue as defined by Eq. (4) and the spin scale T_S as a function of chemical potential. The data is extracted from simulations at $N_c = 8$ and $\beta t = 20$.

we have computed the local spin susceptibility on the cluster, as defined by

$$\chi_f(i\Omega_m) = \frac{1}{L_c^2} \sum_{\mathbf{x}} \int_0^\beta d\tau e^{i\Omega_m \tau} \langle \mathbf{S}_f(\mathbf{x}, \tau) \cdot \mathbf{S}_f(\mathbf{x}) \rangle. \quad (5)$$

Below the coherence temperature, $\chi_f(i\Omega_m = 0)$ is expected to be temperature independent. On the other hand, in the temperature region $T_{\text{coh}} < T \ll U$, it should exhibit Curie-Weiss behavior—the signature of local moment formation. Precisely this behavior is seen in Fig. 5. As the chemical potential grows from $\mu = -2.5t$ to $\mu = -1.875t$, the crossover temperature scale between the Curie-Weiss-like and temperature-independent $\chi_f(i\Omega_m = 0)$ tracks the decrease of the inverse effective mass and coherence temperature. Beyond the phase transition, $\mu = -1.75t > \mu_c$, only Curie-Weiss behavior is apparent in the considered temperature range.

Fig. 6 shows that the band-selective Mott transition is linked to a *sudden* growth of the antiferromagnetic correlations between nearest-neighbor f fermions and to a decrease in the intracell c - f spin-spin correlations. This data supports the picture that, in the band-selective Mott insulating phase, the f quasiparticles are bound into spin singlets amongst themselves. The *gapping* of the spin and charge degrees of freedom of the f quasiparticles at $\mu > \mu_c$ allows for the decoupling of f and c quasiparticles: a c quasiparticle at the Fermi level cannot scatter off an f quasiparticle due to the absence of phase space.

The local dynamical spin structure factor,

$$S_f(\omega) = \text{Im} \frac{\chi_f(\omega)}{1 - e^{-\beta\omega}}, \quad (6)$$

(see Fig. 6) shows a depletion of spectral weight at low energies on both sides of the transition and a considerable sharpening of the line shape in the band-selective

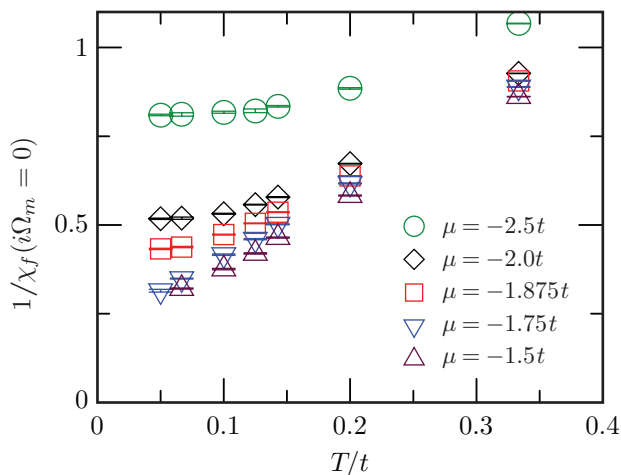


FIG. 5: Inverse local spin susceptibility as a function of temperature for the $N_c = 8$ cluster.

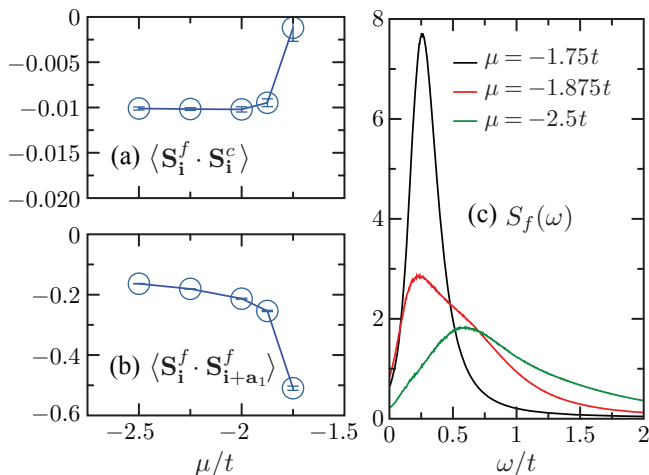


FIG. 6: (a) Intracell spin-spin correlations between c and f fermions. (b) Nearest-neighbor spin-spin correlations between f fermions. (c) Local dynamical spin structure factor.

Mott insulating state. At $\mu < \mu_c$, we can interpret the

data within an itinerant fermion picture where the mass enhancement prior to the band-selective Mott transition is taken into account by a renormalization of the hybridization V and hopping t_f as in a slave boson approach [5]. Following this modeling, the peak position in $S_f(\omega)$, which we will denote by T_S , is expected to track the coherence temperature or, equivalently, the inverse effective mass. The quantity T_S is plotted in Fig. 4 alongside $Z(\mathbf{k}_f)$ and confirms the above expectations to a good degree. At $\mu > \mu_c$, $S_f(\omega)$ should be interpreted within a localized f fermion picture, in which case the peak position is a measure of the excitation energy required to break the singlet state of the f fermions.

We can summarize our results using the terminology of heavy fermions [13]. The band-selective Mott transition corresponds to a Kondo breakdown in which the f fermions drop out of the Luttinger volume. Within our model, it appears that this transition is first order: the reduction of the coherence temperature and the enhancement of the effective mass is interrupted by the formation of a *spin gapped* Mott insulating state of the f fermions. The nature of this band-selective Mott insulating state is very dependent on the cluster topology. In this work, we have considered only clusters with an even number of unit cells—thereby implicitly allowing for spin gapped insulating states of the f fermions within the CDMFT calculation. Despite the breaking of translation invariance inherent to the CDMFT, the Luttinger sum rule still holds when formulated in the Brillouin zone of the supercell Bravais lattice. We can only speculate as to the nature of this state when the cluster size diverges, but we cannot exclude the intriguing possibility that it smoothly connects to fractionalized Fermi liquids [14, 15] with no lattice and spin symmetry breaking but a Luttinger volume encompassing only the c fermions.

Acknowledgments. The numerical calculations were carried out at the LRZ-Münich and the Jülich Supercomputing center. We thank those institutions for their generous allocation of CPU time. KSDB thanks the Humboldt foundation for financial support as well as the FFA and DFG under grant number AS120/4-2.

[1] A. Casey, H. Patel, J. Nyéki, B. P. Cowan, and J. Saunders, Phys. Rev. Lett. **90**, 115301 (2003).
 [2] D. Vollhardt, Rev. Mod. Phys. **56**, 99 (1984).
 [3] M. Imada, A. Fujimori, and Y. Tokura, Rev. Mod. Phys. **70**, 1039 (1998).
 [4] M. Neumann, J. Nyéki, B. Cowan, and J. Saunders, Science **317**, 1356 (2007).
 [5] A. Benlagra and C. Pépin, Phys. Rev. Lett. **100**, 176401 (2008).
 [6] A. Benlagra and C. Pépin, Phys. Rev. B **79**, 045112 (2009).
 [7] G. Biroli, O. Parcollet, and G. Kotliar, Phys. Rev. B **69**, 205108 (2004).

[8] A. W. Sandvik, Phys. Rev. B **57**, 10287 (1998).
 [9] K. S. D. Beach, arXiv:cond-mat/0403055v1 (2004).
 [10] B. Kyung, Phys. Rev. B **75**, 033102 (2007).
 [11] K. S. D. Beach and F. F. Assaad, to be published.
 [12] H. Eskes, M. B. J. Meinders, and G. A. Sawatzky, Phys. Rev. Lett. **67**, 1035 (1991).
 [13] H. v. Löhneysen, A. Rosch, M. Vojta, and P. Wölfle, Rev. Mod. Phys. **79**, 1015 (2007).
 [14] T. Senthil, S. Sachdev, and M. Vojta, Phys. Rev. Lett. **90**, 216403 (2003).
 [15] T. Senthil, M. Vojta, and S. Sachdev, Phys. Rev. B **69**, 035111 (2004).
 [16] The fact that $\langle \hat{n}_f \rangle$ remains less than unity has been con-

firmed by calculations on smaller four-sites clusters, for which lower temperatures can be reached at $\mu > \mu_c$.